NANO LETTERS

Letter

pubs.acs.org/NanoLett

Creation and Control of Two-Dimensional Electron Gas Using Al-Based Amorphous Oxides/$SrTiO_3$ Heterostructures Grown by Atomic Layer Deposition

Sang Woon Lee,[†] Yiqun Liu,[†,‡] Jaeyeong Heo,[†,§] and Roy G. Gordon*[,†]

[†]Department of Chemistry and Chemical Biology, Harvard University, Cambridge, Massachusetts 02138, United States

[‡]GLOBALFOUNDRIES, Inc., Malta, New York 12020, United States

[§]Department of Materials Science and Engineering, Chonnam National University, Gwangju, 500-757, Korea

S *Supporting Information*

ABSTRACT: The formation of a two-dimensional electron gas (2-DEG) using $SrTiO_3$ (STO)-based heterostructures provides promising opportunities in oxide electronics. We realized the formation of 2-DEG using several amorphous layers grown by the atomic layer deposition (ALD) technique at 300 °C which is a process compatible with mass production and thereby can provide the realization of potential applications. We found that the amorphous $LaAlO_3$ (LAO) layer grown by the ALD process can generate 2-DEG (~$1 \times 10^{13}/cm^2$) with an electron mobility of 4–5 $cm^2/V{\cdot}s$. A much higher electron mobility was observed at lower temperatures. More remarkably, amorphous $YAlO_3$ (YAO) and Al_2O_3 layers, which are not polar-perovskite-structured oxides, can create 2-DEG as well. 2-DEG was created by means of the important role of trimethylaluminum, Me_3Al, as a reducing agent for STO during LAO and YAO ALD as well as the Al_2O_3 ALD process at 300 °C. The deposited oxide layer also plays an essential role as a catalyst that enables Me_3Al to reduce the STO. The electrons were localized very near to the STO surface, and the source of carriers was explained based on the oxygen vacancies generated in the STO substrate.

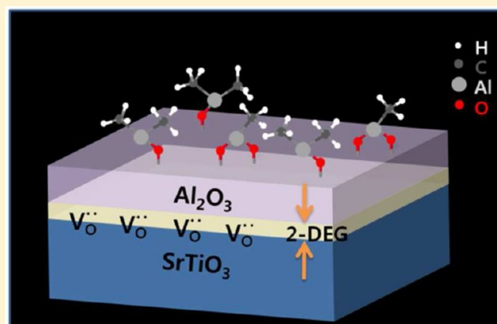

KEYWORDS: *2-D electron gas, amorphous, $LaAlO_3$, Al_2O_3, $SrTiO_3$, atomic layer deposition (ALD), oxygen vacancy*

Heterostructures between complex oxide layers are emerging as interesting systems for oxide electronics due to their unique properties.[1] Ohtomo reported the existence of a two-dimensional electron gas (2-DEG) at the heterointerface between the two insulating oxides $LaAlO_3$ (lanthanum aluminate, LAO) and $SrTiO_3$ (strontium titanate, STO).[2] The LAO films were grown by pulsed laser deposition (PLD) or molecular beam epitaxy (MBE) on a single crystalline (001) STO substrate.[2−8] Transistor-like devices using these LAO/STO heterostructures have also been demonstrated.[3] The most common explanation of the observation of 2-DEG at the LAO/STO interface was based on electronic reconstruction, where the electrons move to the interface to avoid the potential divergence caused by the polar catastrophe.[9] The interface charges are compensated by Ti^{3+} ions that provide electrons to the STO conduction band, and these interface electrons are localized near the $AlO_2/LaO/TiO_2$ interface, which is called an n-type interface. Basically, this electronic reconstruction can only be realized at a well-prepared abrupt and sharp epitaxial interface between single crystalline LAO and STO. An alternative explanation for the generation of 2-DEG is La interdiffusion through the interface, doping the surface layer of the STO to be n-type.[10] A third explanation is defect generation such as oxygen vacancies in the STO substrate.[10−12] Recently, it has been discussed that the oxygen vacancies can be generated at the STO substrate during the growth of the LAO layer as the possible origin of the carrier source.[13,14] In the mean time, the formation of oxygen vacancies has been also supported by theoretical first-principle calculations.[15,16]

Strontium titanate is well-known as a high-*k* dielectric (bulk dielectric constant of 300) with a bandgap of 3.2 eV which has been extensively studied for possible use in electronic devices such as dynamic random access memory (DRAM). Strontium titanate has a cubic perovskite structure with a lattice constant of 0.3905 nm. Lanthanum aluminate is a wide bandgap insulator (5.6 eV) which has a quasi-cubic structure with a lattice constant of 0.3789 nm; thus the lattice mismatch between STO and LAO is small (~3%).[2]

Up to now, epitaxially grown LAO films have been necessary for the creation of 2-DEG. The epitaxial LAO films were grown on an STO substrate by the PLD process at a relatively high growth temperature (650–850 °C)[2−7,9,11−14,17−20] which is one of the representative physical vapor deposition (PVD) techniques. However, the feasibility of an amorphous layer is rarely reported, except in a recent study using amorphous layers grown by the PLD process at room temperature.[13] Unfortu-

Received: June 12, 2012
Revised: August 6, 2012
Published: August 21, 2012

 © 2012 American Chemical Society dx.doi.org/10.1021/nl302214x | *Nano Lett.* 2012, 12, 4775−4783

nately, the PLD process has a lower chance of being used in the mass production of devices.

ALD is characterized by its unique self-limiting growth mechanism based on alternating saturated surface reactions. The precursor and oxygen source are pulsed into a reactor alternately, and each injection is separated by a purging process using inert gas.[21] This process provides a lot of advantages in terms of excellent conformality and precise control of thickness as well as large area uniformity. In practice, the ALD process is being widely used for the growth of dielectric films in the mass-production of microelectronic devices.[21]

In this paper, a practical, novel technique is proposed to create and control 2-DEG using several amorphous films on STO substrates in which oxygen vacancies act as the source of the carriers. An amorphous LAO layer grown by an ALD process creates 2-DEG by generating oxygen vacancies in the STO substrate. More remarkably, amorphous Al_2O_3 as well as $YAlO_3$ (YAO) grown by ALD on STO substrates, which are not polar-perovskite structured oxides, can create 2-DEG at the interface. The aluminum source for these ALD processes, trimethylaluminum (TMA), creates oxygen vacancies in the STO substrate during the growth of several aluminum-containing layers, including amorphous LAO, YAO and Al_2O_3. However, treatment with TMA vapor alone does not create any oxygen vacancies. The presence of a growing oxide layer (LAO, Al_2O_3, $YAlO_3$, etc.) produced by water vapor as a co-reactant is also needed to catalyze the reduction. 2-DEG density was controlled precisely and reproducibly, which indicates that the formation of oxygen vacancies was well-controlled by the ALD process. Growth of other oxides not containing Al, such as Y_2O_3, La_2O_3, or $LaYO_3$, did not produce 2-DEG.

All films used in this experiment, including the LAO layer, were grown by ALD at 300 °C. The ALD technique enabled the formation of smooth and high quality oxide thin films at a low growth temperature (300 °C) with atomic precision, which is essential to the functionality of oxide heterostructures. The Al_2O_3 ALD process offers great advantages in terms of mass production compatibility due to its ideal ALD reaction.[22] The growth of an amorphous layer is easy to achieve by the ALD process with a large process margin; thus it is promising for the realization of potential applications.

Results and Discussion. Figure 1a shows the cross-sectional high-resolution transmission electron microscopy (TEM) image of the LAO layer grown by ALD at 300 °C on an STO substrate. The amorphous LAO layer grown on a single crystalline STO substrate is clearly observed. Figure 1b shows the [001] zone axis electron diffraction pattern at the interfacial region of the LAO/STO heterostructure. The diffraction pattern consists of single spots, and those diffraction spots are exactly consistent with those of single crystalline STO,[23] which indicates that the STO substrate used in this experiment is a perfect single crystalline material. However, no diffraction spots were observed from the LAO layer, which confirms the amorphous nature of the LAO layer.

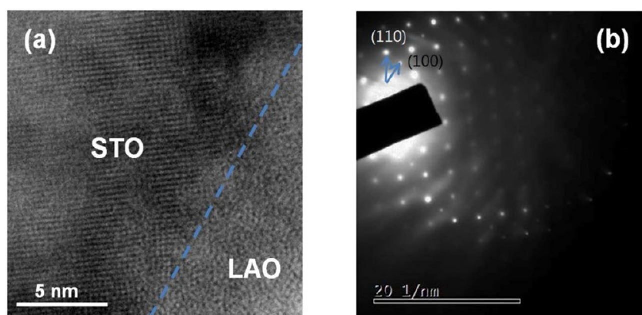

Figure 1. (a) Cross sectional high-resolution TEM image of LAO/STO showing amorphous LAO layer grown on a single crystalline STO substrate. (b) [001] zone axis electron diffraction pattern at the interfacial region of the LAO/STO heterostructure.

The surface morphologies of the samples were investigated by means of an atomic force microscope (AFM). Figure 2a shows the surface morphology of a TiO_2-terminated STO substrate.[24,25] The surface consists of regular terrace structures with a high smoothness (rms roughness of 0.15 nm). The height difference between the adjacent terraces is about 0.4 nm which corresponds to one unit-cell of STO as shown in Figure 2b. Figure 2c shows the surface morphology of a 6 nm thick-LAO film grown on an STO substrate by the ALD process at 300 °C. The roughness of the LAO surface (about 0.2 nm) is slightly higher than that of the STO substrate. The background terrace structure was preserved, although the LAO film was grown on an STO substrate. This result implies that LAO films grown by ALD are very smooth, replicating the underlying terrace structure. Figure 2d shows the sheet resistance (R_s) and sheet carrier density (n_s) as a function of the amorphous LAO film thickness grown on the STO substrate (LAO/STO heterostructure). A stoichiometric (51.4 at. % of La) LAO film was grown by an ALD cycle ratio of 2:1 (La:Al) as confirmed by RBS (Figure S1a), and the thicknesses of the films grown on the STO substrate were estimated by an X-ray reflectivity (XRR) measurement (Figure S2). Even with amorphous LAO films, the carriers can be created, and a critical thickness exists which is required to make the channel to be conducting. The insulating interface of the LAO/STO heterostructures becomes conducting above a LAO thickness of ~3 nm, and the sheet resistance and sheet carrier density remain constant above this critical thickness. Here, the type of carrier is an electron according to the sign of the Hall voltage. This transition behavior of the amorphous LAO/STO heterostructure is similar to the epitaxial LAO/STO heterostructure.[3,6] The critical thickness of ~3 nm is somewhat thicker than the commonly reported value (~4 unit cells) from the epitaxial LAO films grown by PLD.[3] The sheet resistance and sheet carrier density of the amorphous LAO/STO heterostructures were $\sim 1 \times 10^5$ Ω/sq. and $\sim 1 \times 10^{13}/cm^2$, respectively, where the mobility was 4−5 $cm^2/V \cdot s$ as shown in Figure 2e, whereas those of the insulating heterostructures were $>10^9$ Ω/sq. and $<10^9/cm^2$ which are beyond the sensitivity of the measurement.

Astonishingly, the 2-DEG can be generated by depositing an amorphous Al_2O_3 layer as well as a YAO layer on the STO substrate as shown in Figure 3. Figure 3a shows the schematic diagram of several heterostructures using various oxide layers. The sheet resistance and carrier density of the YAO/STO heterostructure were almost identical with those of the LAO/STO heterostructure as shown in Figure 3b. The sheet resistance of the Al_2O_3/STO heterostructure is slightly higher than that of the STO/LAO heterostructure by a factor of 3 because of the reduced carrier density ($\sim 3 \times 10^{12}/cm^2$). However, the 2-DEG was not generated by depositing amorphous La_2O_3, Y_2O_3, or $LaYO_3$ (LYO) layers on an STO substrate at 300 °C by ALD as shown in Figure 3b. The basic crystal structure of YAO is an orthorhombic, a space group P_{nma}

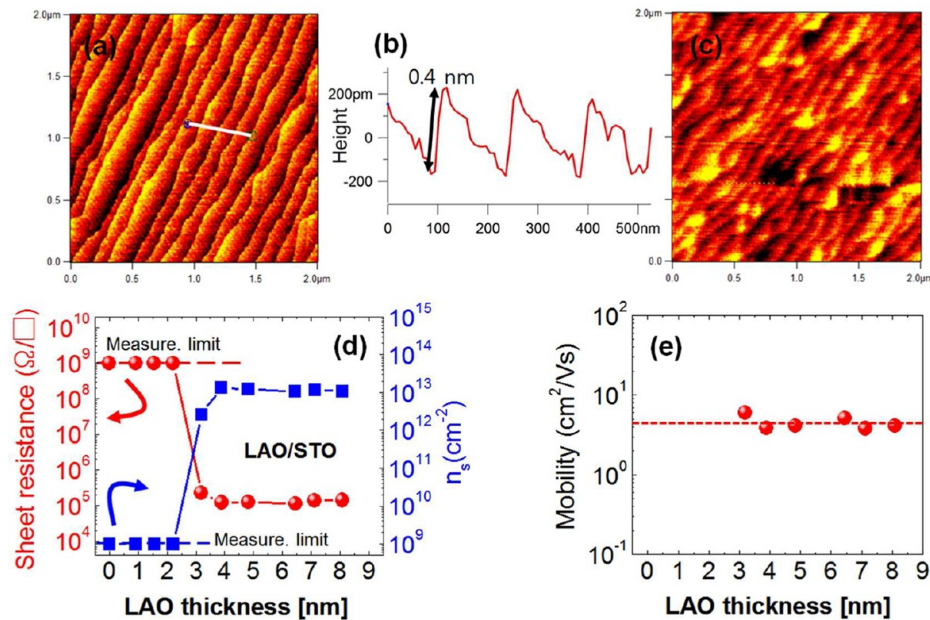

Figure 2. (a) Surface morphology of the TiO_2-terminated STO substrate by AFM, which consists of regular terrace structures with a quite smooth flatness (rms roughness of 0.15 nm). (b) The height difference between adjacent terraces corresponds to one unit-cell of STO (~0.4 nm). (c) The surface morphology of a 6 nm thick-LAO film grown on an STO substrate by ALD at 300 °C (rms of 0.2 nm). (d) The sheet resistance and sheet carrier density and (e) mobility as a function of the amorphous LAO film thickness grown on an STO substrate.

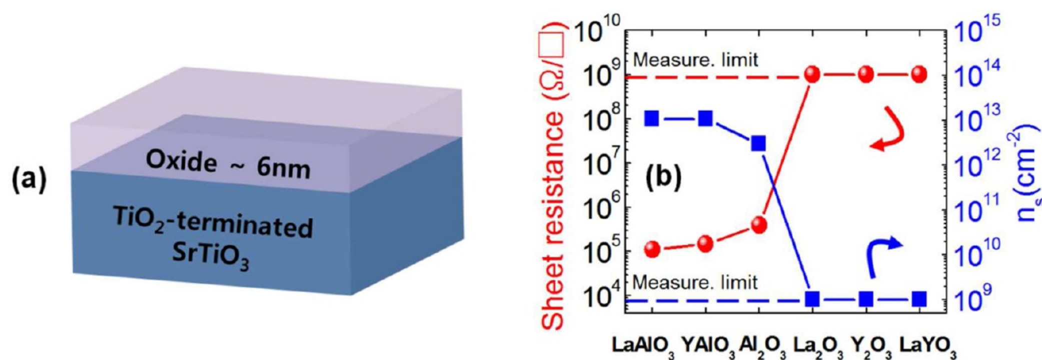

Figure 3. (a) Schematic of several heterostructures using various oxide layers. (b) The sheet resistance and carrier density of several heterostructures showing that 2-DEG can be generated by depositing an amorphous LAO, YAO, and Al_2O_3 layer on an STO substrate but that La_2O_3, Y_2O_3, and $LaYO_3$/STO did not generate any conductivity.

(space group number 62), which lattice constants are: a = 0.5330 nm, b = 0.7375 nm, and c = 0.5180 nm.[26] This is a small distortion of the perovskite unit cell. However, it should be noted that Al_2O_3 is not a polar-perovskite structured oxide with cubic or distorted cubic unit cells. Instead, crystalline Al_2O_3 can be described by trigonal or hexagonal unit cells (space group number 167), while ALD Al_2O_3 is amorphous.

Figure 4a shows the sheet resistance and sheet carrier density of an Al_2O_3/STO heterostructure as a function of Al_2O_3 film thickness when Al_2O_3 is grown on a STO substrate. The sheet resistance decreased sharply, and the sheet carrier density increased abruptly above an Al_2O_3 thickness of 1.2 nm. Then the sheet resistance and sheet carrier density remained constant above this critical thickness. The sheet resistance and sheet carrier density of the conducting heterostructure are 4×10^5 Ω/sq. and $\sim 3 \times 10^{12}$/cm^2, respectively. The carrier density of the Al_2O_3/STO heterostructure is slightly lower than that of the LAO/STO heterostructure ($\sim 1 \times 10^{13}$/cm^2) as mentioned earlier. The mobility was constant regardless of the Al_2O_3 film thickness (Figure S3a).

Figure 4b shows the sheet resistance and sheet carrier density of the LAO/Al_2O_3/STO heterostructure as a function of Al_2O_3 film thickness when the Al_2O_3 film was grown prior to the growth of the LAO film. Six nm-thick LAO films were grown on top of Al_2O_3 films to fabricate the LAO/Al_2O_3/STO heterostructures. The sheet resistance and created carrier density of the LAO/Al_2O_3/STO heterostructure were identical to those of the Al_2O_3/STO heterostructure, which suggests the creation of the 2-DEG was determined by the Al_2O_3 layer, not by the LAO layer. The mobility was constant irrespective of the Al_2O_3 film thickness (Figure S3a).

Figure 4c shows the sheet resistance and sheet carrier density of the YAO/STO heterostructure as a function of YAO film thickness. The stoichiometric (51.3 at. % of Y) YAO film was grown by an ALD cycle ratio (Y:Al) of 2:1 as confirmed by Rutherford backscattering spectroscopy (RBS) (Figure S1b). The transition behaviors of the resistance, carrier density and mobility depending on the film thickness are almost identical with the LAO/STO heterostructure as shown in Figure 2d. However, the insulating interface of the YAO/STO hetero-

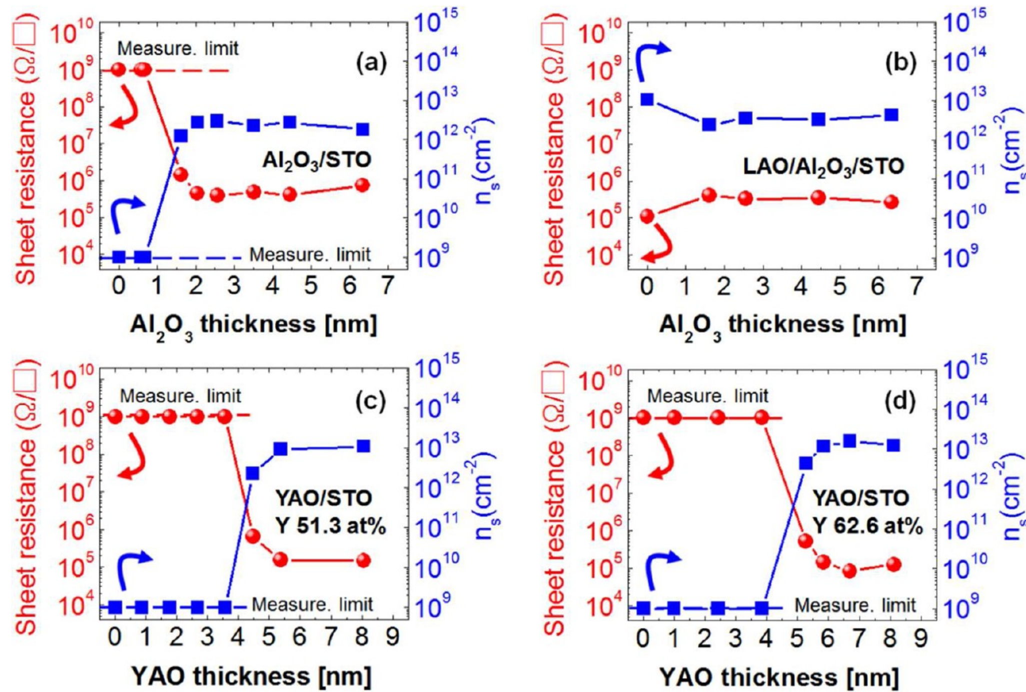

Figure 4. Sheet resistance and sheet carrier density of (a) Al_2O_3/STO and (b) LAO/Al_2O_3/STO heterostructures as a function of Al_2O_3 film thickness. Six nm-thick LAO films were grown on top of Al_2O_3 films in part (b). The sheet resistance and sheet carrier density of (c) stoichiometric (51.3 at. % of Y) YAO/STO and Y-rich (62.6 at. % of Y) YAO/STO heterostructures as a function of the YAO film thickness. YAO films were grown by ALD using cycle ratios of 2:1 (Y:Al) and 4:1, respectively.

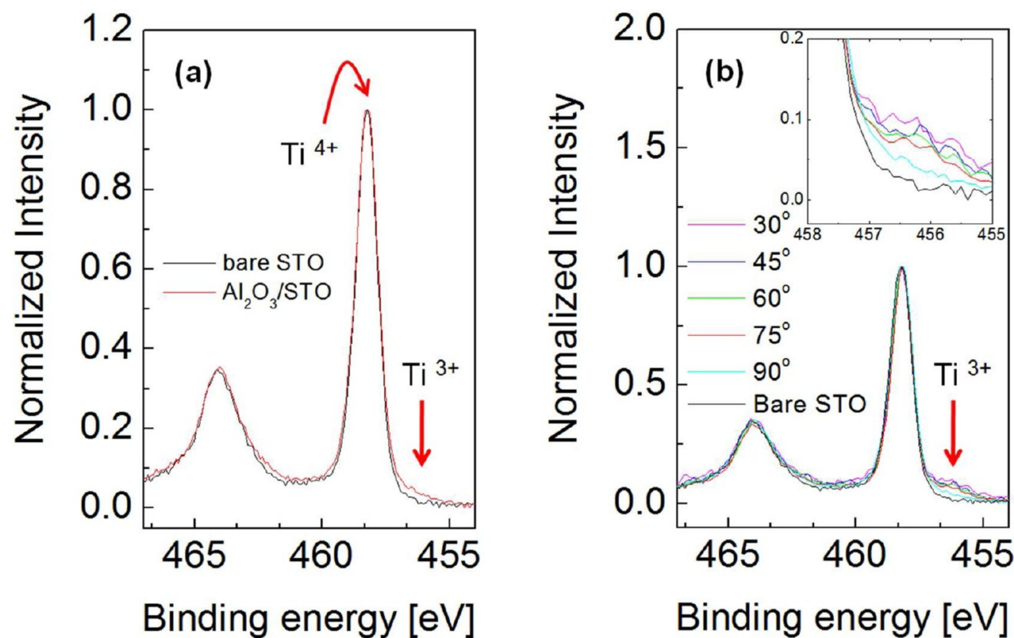

Figure 5. (a) Normalized Ti 2p spectra of a 2.5 nm-thick Al_2O_3/STO heterostructure measured by normal XPS showing more increased Ti^{3+} signal (~456.2 eV) with Al_2O_3/STO heterostructure than the bare STO substrate, which indicates the generation of oxygen vacancies in STO during the growth of the Al_2O_3 layer by ALD. The signal from the bare STO substrate was used for comparison. (b) Normalized Ti 2p spectra of a 2.5 nm-thick Al_2O_3/STO heterostructure obtained by angle-resolved XPS showing that the carriers are localized at the interface, where all of the spectra were normalized to have the same Ti^{4+} peak height.

structure becomes conducting above a YAO thickness of ~4 nm. The critical thickness of ~4 nm for YAO is thicker than that of the LAO/STO heterostructure.

All of these layers are amorphous as confirmed by TEM and X-ray diffraction (XRD) (Figure S4), so the polar catastrophe mechanism can be ruled out as the explanation for the formation of 2-DEG in our heterostructures. The possibility of a La ion doping into the STO substrate was ruled out because the 2-DEG was not generated when the single layer of La_2O_3 was grown on the STO substrate. It has been reported that La atoms can replace Sr sites in STO to generate electrons by La_{Sr} substitution;[27,28] however, this phenomenon was not observed

in this work. The possibility of an Al ion doping into the STO substrate can also be excluded because it is known that Al atoms are prone to replace Ti sites, where Al atoms can act as acceptors.[29−31] The substituted Al atoms in Ti sites reduce the density of electrons, so that the Al doping technique has been used to reduce the carriers in TiO_2-based dielectric materials. The chance of a Y ion doping into the STO substrate was also excluded, as well as La ion doping, for the same reason.

The likely origin of the free electrons is the creation of oxygen vacancies in the STO during the growth of aluminum-containing oxides such as LAO, YAO and Al_2O_3. The possibility of reduction of the STO substrate prior to the deposition of each film can be excluded. It has been reported that the STO substrate is reduced at a growth temperature of 800 °C and low oxygen pressure of 10^{-6} mbar without the actual deposition of an LAO film grown by PLD due to high growth temperature and low oxygen pressure.[14] Basically, the STO substrate used in our experiment is insulating ($R_s > 10^9$ Ω/sq.) before the deposition of the oxides, and the STO substrate still keeps its insulating property even in the chamber without actual growth of the film for a few hours. Also a STO substrate keeps its insulating property even after an exposure of the STO substrate to TMA molecules (see Figure S6 and Supporting Information).

The observation of the Ti^{3+} binding state from the Ti 2p core-level spectrum can provide direct evidence of oxygen vacancies in the STO. X-ray photoelectron spectroscopy (XPS) measurements were performed to determine the valence state of Ti as shown in Figure 5. Figure 5a shows the normalized Ti 2p spectra of a 2.5 nm-thick Al_2O_3/STO heterostructure, and the signal from the bare STO substrate was used for comparison. An increased Ti^{3+} signal at ∼456.2 eV was observed in the Al_2O_3/STO heterostructure compared to the bare STO substrate, which means that the oxygen vacancies were generated in the STO during the growth of the Al_2O_3 layer by ALD. For the estimation of the Ti^{3+} depth profile, angle-resolved XPS was measured with various photoelectron takeoff angles with a 2.5 nm-thick Al_2O_3/STO heterostructure as shown in Figure 5b. The effective electron escape depth decreases with decreasing the takeoff angle; thus the XPS spectrum becomes more surface-sensitive (Figure S5). The signal of Ti^{3+} relative to the Ti^{4+} main line increases as the takeoff angle decreases. This indicates that the electrons generated by oxygen vacancies are localized at the STO surface region as a 2-DEG (within ∼2 nm from the interface), which is smaller than the electron escape depth (∼5 nm, see Supporting Information).

The mobilities of all conducting heterostructures (∼5 cm^2/V·s) are consistent with generally reported values of reduced STO having many oxygen vacancies.[11] The carriers of all heterostructures disappeared after annealing at 600 °C for 1 h in an oxygen atmosphere. The carriers disappeared even after annealing at 300 °C for 1 h in an oxygen atmosphere. These facts provide additional evidence that the source of the carriers was generated by oxygen vacancies on the STO side.

The transfer of the oxygen between LAO and STO has been experimentally reported during the growth of each oxide grown by PLD using an ^{18}O isotope by means of dynamic secondary ion mass spectroscopy (D-SIMS).[17] Oxygen transfer was observed at a high growth temperature (750 °C) as the thick LAO film (>50 nm) was grown on the STO substrate. However, the oxygen transfer was significantly reduced as the growth temperature decreased below 650 °C.

When it comes to the ALD process, oxygen transfer and reduction of the substrate is also possible provided the thermodynamic condition is satisfied and the reaction kinetics are fast enough. The metal precursor molecules are introduced on the substrate separately without overlapping the oxygen source in the ALD process. Usually, these metal precursor molecules tend to be oxidized by scavenging the nearby oxygen.[32] The substrate material was reduced during the pulse of the metal precursor without introducing an oxygen source, such as an H_2O or O_3 vapor, by means of oxidation of the metal precursor.[32] However, the kinetics of the redox reaction can be limited by the low growth temperature of ALD and the strong bond of complex ligands attached to the metal precursor molecules in the ALD reaction.

The Gibbs free energy of reaction (ΔG_r) can indicate whether the reduction of the STO substrate by TMA during the Al_2O_3 ALD process is feasible.[33−35] Possible overall reactions for the reduction of the STO substrate by the TMA at 573 K are the following:

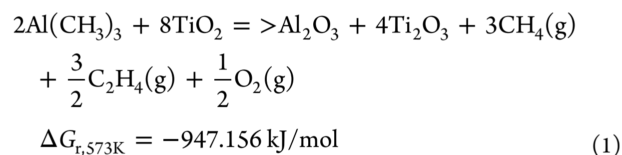

$$2Al(CH_3)_3 + 8TiO_2 => Al_2O_3 + 4Ti_2O_3 + 3CH_4(g) + \frac{3}{2}C_2H_4(g) + \frac{1}{2}O_2(g) \quad \Delta G_{r,573K} = -947.156\ kJ/mol \tag{1}$$

or

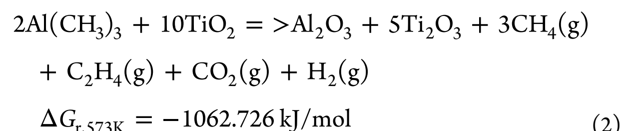

$$2Al(CH_3)_3 + 10TiO_2 => Al_2O_3 + 5Ti_2O_3 + 3CH_4(g) + C_2H_4(g) + CO_2(g) + H_2(g) \quad \Delta G_{r,573K} = -1062.726\ kJ/mol \tag{2}$$

The reaction pathways were expected based on the reports that CH_4 gas was mainly produced with small amounts of C_2H_4 and CO_2 gases as byproducts when TMA dissociates in the presence of oxygen during the Al_2O_3 ALD process.[36,37] The change in Gibbs free energies (ΔG_r) is negative for reaction pathways (1) and (2) because of the formation of strong Al−O bonds. Thus, at equilibrium, the oxidation of TMA molecules can drive a thermodynamically favorable reduction of STO substrates.[38,39] Of course, other gaseous byproducts, such as CO or H_2CO, are also possible, but large negative free energy changes also favor these reactions going to completion at equilibrium.

In one experiment, reduction of the STO by the injection of TMA alone did not occur, which means that the thermal energy was not enough to overcome the activation energy due to the slow kinetics at a reaction temperature of 300 °C, even though the thermodynamic condition was satisfied. However, reduction of the STO did happen when LAO, YAO and Al_2O_3 films were thicker than their critical thicknesses. As a result, the repetitive pulse (55 cycles) of the Al precursor, TMA, which was used for the deposition of the LAO, YAO and Al_2O_3 films, on the STO substrate without introducing an oxygen source (H_2O) did not induce the reduction of the STO substrate at 300 °C because of the absence of the LAO, YAO and Al_2O_3 layers. This is also the case when the repetitive pulses (55 cycles) of TMA are applied to the Y_2O_3 layers previously grown on the STO substrate, irrespective of the Y_2O_3 film thickness (Figure S6a). It should be noted that the interface of the Y_2O_3/STO heterostructure is insulating as shown in Figure 3b. In this case, the carriers were generated by means of following the deposition of a 6 nm-thick LAO layer on top of the Y_2O_3/STO heterostructure as shown

in Figure S6a. There still exists a required critical thickness of LAO and Al_2O_3 layers when those layers are grown on top of the Y_2O_3 layer (4.7 nm-thick) to create carriers, which emphasizes the important role of pre-grown LAO and Al_2O_3 layers (Figure S6b). LAO and Al_2O_3 layers that are thicker than the critical thickness are necessary for the redox reaction even on the Y_2O_3/STO heterostructure; thus reduction of the STO can occur during the metal precursor pulse. As discussed above, the carriers were generated only after growing a certain thickness LAO (>3 nm), YAO (>4 nm) and Al_2O_3 (>1.2 nm) layers on the STO substrate at 300 °C. An important feature is that the Al_2O_3 component is always included in those oxides, such as LAO, YAO, and Al_2O_3, which generated the carriers in an interaction with the STO. Here, we claim that Al_2O_3 (>1.2 nm) acts as a catalyst for the reaction; thus the redox reaction of the STO substrate can occur when the TMA molecules are introduced. The Al_2O_3 layer (>1.2 nm) promoted the kinetics of the redox reaction. Therefore, the redox reaction is strongly enhanced at the interface, which results in the oxygen vacancies generated on the STO surface by means of the TMA molecules' oxidation at 300 °C. The minimum required Al_2O_3 amount for the carrier generation was estimated by ~15 cycles of Al_2O_3 ALD, which corresponds to a 1.35 nm-thick Al_2O_3 layer. An important fact suggesting that this redox reaction is limited by kinetics is that the carrier density decreased significantly with the decreasing growth temperature (Figure S7). The carrier density was decreased by a factor of 10^3 at a growth temperature of 250 °C; it could not be measured at 200 °C due to the measurement limit (decreased by a factor of $>10^4$).

It is understood that the outward diffusion of oxygen owing to the redox reaction of the STO is limited by grown oxides such as the LAO, YAO and Al_2O_3 layers due to their diffusivity of oxygen. The outward diffusion of oxygen from the interface of the heterostructure would be limited by those oxides; thus, the carrier density does not increase above the critical thickness. This is an interesting feature in terms of the self-limiting control of the carrier by outward diffusion of oxygen in the redox reaction. It has been reported that metallic species such as Al, Ti, Y, Ba and Zr can interact with the STO substrate at room temperature, which indicates the interfacial redox reaction occurs, and the interactions happen at the STO surfaces.[13,35]

Based on the above discussion, we expected that the carriers would be generated even though the composition of the YAO layer is varied far from the stoichiometry, as long as the amount of the Al_2O_3 component in the YAO layer is enough (> ~15 cycles). Figure 4d shows the sheet resistance and carrier density depending on the Y-rich YAO layer thickness. A Y-rich YAO (62.6 at. % of Y) film was grown by an ALD cycle ratio (Y:Al) of 4:1 as determined by RBS (Figure S1c). Although the composition of the YAO layer is out of the stoichiometric range, the transition behavior was also observed. This result supports that the creation of 2-DEG does not originate from the perovskite nature of the YAO layer. The insulating interface of the YAO/STO heterostructure becomes conducting above the YAO thickness of ~4.5 nm. The critical thickness of ~4.5 nm is a little bit thicker than the stoichiometric YAO/STO heterostructure (~4 nm). A Y-rich YAO film (4 Y_2O_3 cycles per Al_2O_3 cycle) is thicker than a stoichiometric YAO film (2 Y_2O_3 cycles per Al_2O_3 cycle) because more Y_2O_3 ALD cycles are included as the same Al_2O_3 cycles in Y-rich YAO ALD than in stoichiometric YAO ALD. The minimum required Al_2O_3 cycles in the Y-rich YAO/STO heterostructure for the carrier generation were almost identical (~15 cycles of Al_2O_3 ALD) with the stoichiometric YAO/STO and also with the LAO/STO and Al_2O_3/STO heterostructures, which indicates that the amount of Al_2O_3 in the film is the most important factor of the redox reaction. The creation of 2-DEG during the growth of the Al_2O_3 layer on the STO surface was schematically described according to the above model in Figure 6.

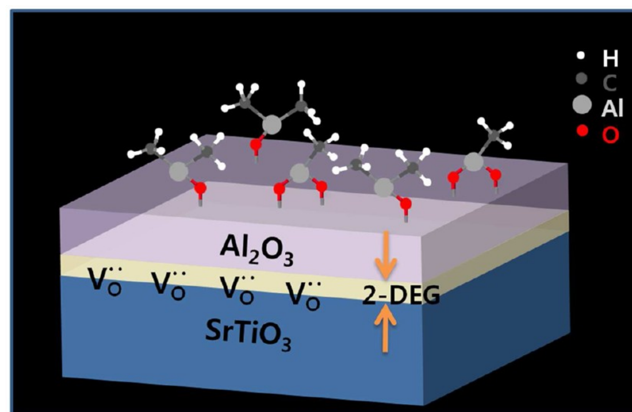

Figure 6. Schematic diagram of 2-DEG creation by the reduction of STO by TMA during the growth of an Al_2O_3 film at 300 °C. The Al_2O_3 layer (>15 cycles of Al_2O_3 ALD) promoted the kinetics of the redox reaction; thus the oxygen vacancies could be generated on the STO surface by oxidation of TMA molecules.

Figures 7a–c show the variation of sheet resistance, mobility and sheet carrier density acquired from Hall measurement results depending on the measurement temperature of the several heterostructures. The sheet resistance variations of all heterostructures were decreased with a decreasing temperature because the mobility increases with a decreasing temperature (Figure 7a). The mobility variations were identical for all heterostructures which indicates the mobilities were governed by the STO, and the increasing mobility with decreasing temperature is a typical property of STO (Figure 7b).[28,40] The mobility was further increased with decreasing temperature down to 30 K (Figure S8). The sheet carrier density of the LAO/STO heterostructure was slowly decreased with decreasing temperature, and the sheet carrier density of the Al_2O_3/STO heterostructure was decreased slightly faster than the LAO-based heterostructure (Figure 7c). However, the insertion of the Y_2O_3 layer between the STO substrates and the LAO or Al_2O_3 films produced a more metallic channel (E_a < 10 meV) where the carrier density was not decreased with decreasing temperature. Figure 7d shows the Arrhenius plot of the sheet carrier densities versus temperature, which gives the activation energy from the slope. The activation energies were close to zero in the LAO/Y_2O_3/STO and Al_2O_3/Y_2O_3/STO heterostructures, which indicates metallic channels were formed. At room temperature, the sheet resistance was even decreased from 1.1×10^5 to 6.72×10^4 Ω/sq. when the Y_2O_3 layer was inserted between the LAO layer and the STO substrate. The sheet carrier density was increased from 1.16×10^{13} to $1.87 \times 10^{13}/cm^2$. The role of Y_2O_3 between LAO and STO is totally different from that of the epitaxially grown STO/Y_2O_3/STO heterostructure, where the single atomic layer of Y_2O_3 induced an insulating interface,[41] because the electronic reconstruction theory does not fit our system. Although the carrier densities decrease slightly with decreasing temperature in the LAO/STO

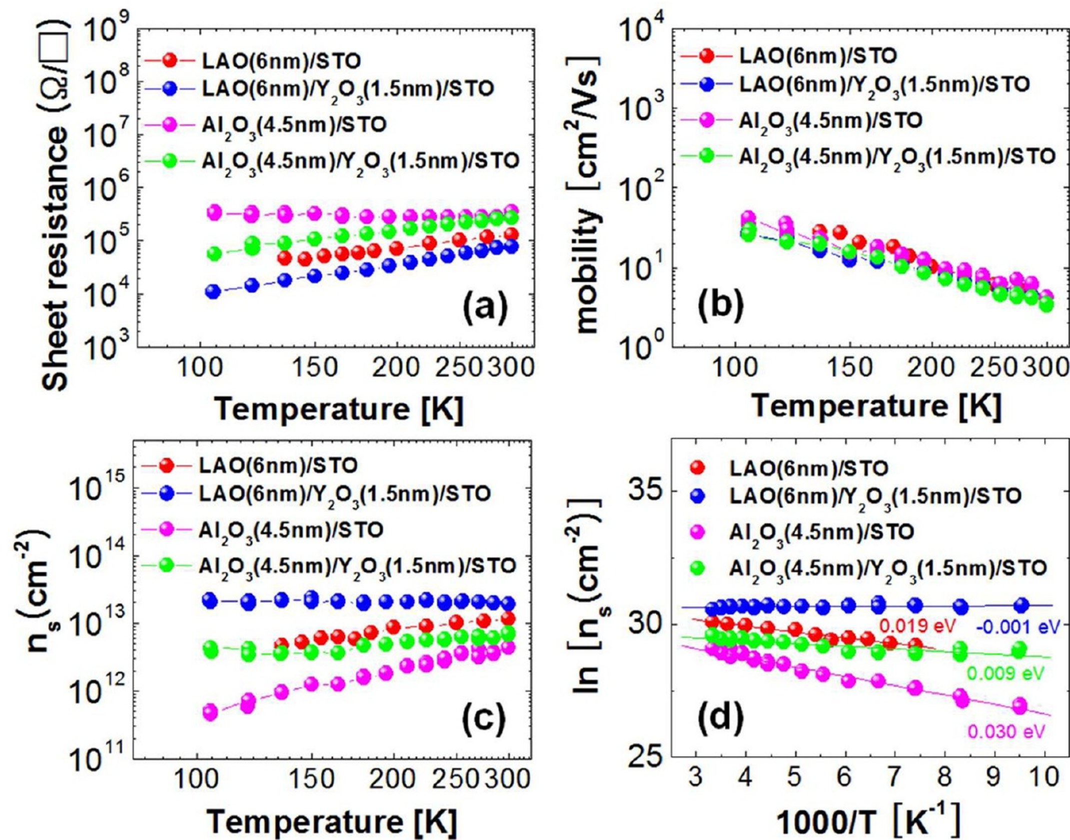

Figure 7. (a−c) Variation of sheet resistance, mobility and sheet carrier density from Hall measurements depending on the measurement temperature of the several heterostructures. (d) Activation energies of the several heterostructures by Arrhenius plotting of the temperature-dependence of the sheet carrier densities, which indicate metallic channels were successfully formed (E_a < 30 meV).

and Al_2O_3/STO heterostructures, the activation energies were very small (E_a < 30 meV) and consistent with the oxygen-deficient STO[42] as shown in Figure 7d which indicates that conducting channels were successfully formed.

Conclusions. Up to now, a physical vapor deposition method, such as PLD, was used to generate 2-DEG to grow an epitaxial LAO film on an STO substrate. Here, we showed that 2-DEG can be created by growing an amorphous LAO layer as well as YAO and Al_2O_3 layers grown by the ALD process on an STO substrate. It was revealed that the key factor for the creation of 2-DEG was an Al_2O_3 ALD process forming oxygen vacancies in the STO by oxidation of the TMA. In practice, the ALD technique has been used for the mass production in the semiconductor field. Among them, the ALD of Al_2O_3 is strongly recommended in the mass production since it is an easy and cheap process with a large processing window and precise atomic level control. The TMA precursor has a very simple structure which can induce an ideal ALD reaction. Eventually, the formation of oxygen vacancies on the STO substrate is well-controlled by the ALD process. These heterostructures fabricated at a low temperature (~300 °C) by ALD provide promising opportunities in oxide electronics. In addition, it can allow more chance to the scalability of a device if the 2-DEG can be created by ALD on the epitaxially grown STO films on SiO_2; likewise the observation of 2-DEG on the epitaxially grown STO films on SiO_2 according to the recent report by Park.[6] Thus, the creation and control of 2-DEG by the ALD technique using a TMA precursor is of great importance in terms of the realization of device fabrication. Further process optimization and theoretical calculations will aid in the achievement of devices with even higher performance.

Methods. *Sample Growth.* LAO films were deposited on TiO_2-terminated (001) STO single crystals purchased from MTI Corporation, and TiO_2-termination was achieved by chemical etching.[24,25] The LAO films were grown at a growth temperature of 300 °C by ALD in a horizontal gas flow reactor at a working pressure of 400 mTorr (base pressure 30 mTorr). All films, including an LAO layer, were grown by ALD at 300 °C. Lanthanum tris(*N*,*N*′-diisopropylformamidinate) (Dow Chemical Company) was used as the La-precursor, and H_2O was used as the oxygen source. TMA (Sigma Aldrich) was used as the Al-precursor, and H_2O was used as the oxygen source for the deposition of Al_2O_3. One super cycle consisted of two subcycles of La_2O_3 and one subcycle of Al_2O_3 for the deposition of the stoichiometric LAO films. A Y_2O_3 thin film was deposited by ALD using yttrium tris(*N*,*N*′-diisopropylacetamidinate) (Dow Chemical Company) and H_2O at a growth temperature of 300 °C. A stoichiometric YAO film (51.3 at. % of Y) was grown with a super cycle ratio of 2:1 (Y:Al), and Y-rich YAO film (62.6 at. % of Y) was grown with a super cycle ratio of 4:1 (Y:Al).

Measurement of Film Properties. The thickness of the film grown on an STO substrate was estimated by X-ray reflectivity (XRR, PANAlytical, X'Pert Pro) measurements using a Cu Kα X-ray source. The amorphous phase of the film was analyzed by high-resolution TEM (HRTEM, JEOL 2010F) and glancing angle X-ray diffraction (GAXRD). The film surface morphology

was investigated by an atomic force microscope (AFM, Asylum, MFP-3D SA). The composition of the film was evaluated by Rutherford backscattering spectroscopy (RBS) using a 2 MeV He^{2+} beam. X-ray photoelectron spectroscopy (XPS, PHI, VersaProbe II) measurements were performed to determine the valence state of the Ti. For the estimation of the Ti^{3+} depth profile, the angle-resolved XPS measurement was examined with various photoelectron takeoff angles. The effective electron escape depth decreases with the decreasing takeoff angle; thus the analysis becomes more surface-sensitive.

Electrical Measurement. For the Hall measurement, four 100 nm-thick Au electrodes (diameter of 1 mm with a 10 nm-thick Ti adhesion layer) were deposited at the corners of 1 cm square samples by e-beam evaporation (Denton) using a shadow mask after the deposition of the thin films onto the STO substrate. Sheet resistance (R_s) and sheet carrier density (n_s) were measured by the Hall measurement system using the Van der Pauw configuration, and the mobility was evaluated from the relationship between R_s and n_s. Ohmic contact property was confirmed by $I-V$ measurement between two Au electrodes (Figure S9). The measuring temperature was controlled by means of vacuum-assisted cooling with the help of liquid nitrogen, which allowed the lowest temperature of 100 K.

■ ASSOCIATED CONTENT

Supporting Information

Termination of STO, thin film growth, composition of amorphous films, estimation of amorphous film thickness, extraction of the mobility, confirmation of the amorphous phase grown on STO substrate, angle-resolved X-ray photoelectron spectroscopy, role of TMA precursor and pre-grown LAO and Al_2O_3 layers, influence of the growth temperature, mobility of LAO/STO at low temperatures, confirmation of ohmic contact, and stability of 2-DEG in the heterostructure. This material is available free of charge via the Internet at http://pubs.acs.org.

■ AUTHOR INFORMATION

Corresponding Author

*E-mail: gordon@chemistry.harvard.edu.

Notes

The authors declare no competing financial interest.

■ ACKNOWLEDGMENTS

The lanthanum and yttrium amidinate precursors were supplied by the Dow Chemical Company. S.W. Lee would like to thank Meng-Ju Sher for assistance with the Hall measurements at low temperatures. This work was performed in part at the Center for Nanoscale Systems (CNS) at Harvard University, a member of the National Nanotechnology Infrastructure Network (NNIN), which is supported by the National Science Foundation under NSF award no. ECS-0335765.

■ REFERENCES

(1) Mannhart, J.; Schlom, D. G. *Science* **2010**, *327*, 1607−1611.
(2) Ohtomo, A.; Hwang, H. Y. *Nature* **2004**, *427*, 423−426.
(3) Thiel, S.; Hammerl, G.; Schmehl, A.; Schneider, C. W.; Mannhart, J. *Science* **2006**, *313*, 1942−1945.
(4) Xie, Y.; Bell, C.; Yajima, T.; Hikita, Y.; Hwang, H. Y. *Nano Lett.* **2010**, *10*, 2588−2591.
(5) Rijnders, G.; Blank, D. H. A. *Nat. Mater.* **2008**, *7*, 270−271.
(6) Park, J. W.; Bogorin, D. F.; Cen, C.; Felker, D. A.; Zhang, Y.; Nelson, C. T.; Bark, C. W.; Folkman, C. M.; Pan, X. Q.; Rzchowski, M. S.; Levy, J.; Eom, C. B. *Nat. Commun.* **2010**, *1*, 94.
(7) Cen, C.; Thiel, S.; Hammerl, G.; Schneider, C. W.; Andersen, K. E.; Hellberg, C. S.; Mannhart, J.; Levy, J. *Nat. Mater.* **2008**, *7*, 298−302.
(8) Segal, Y.; Ngai, J. H.; Reiner, J. W.; Walker, F. J.; Ahn, C. H. *Phys. Rev. B* **2009**, *80*, 241107.
(9) Nakagawa, N.; Hwang, H. Y.; Muller, D. A. *Nat. Mater.* **2006**, *5*, 204−209.
(10) Chambers, S. A. *Adv. Mater.* **2010**, *22*, 219−248.
(11) Herranz, G.; Basletić, M.; Bibes, M.; Carrétéro, C.; Tafra, E.; Jacquet, E.; Bouzehouane, K.; Deranlot, C.; Hamzić, A.; Broto, J. M.; Barthélémy, A.; Fert, A. *Phys. Rev. Lett.* **2007**, *98*, 216803.
(12) Siemons, W.; Koster, G.; Yamamoto, H.; Harrison, W. A.; Lucovsky, G.; Geballe, T. H.; Blank, D. H. A.; Beasley, M. R. *Phys. Rev. Lett.* **2007**, *98*, 196802.
(13) Chen, Y.; Pryds, N.; Kleibeuker, J. e. E.; Koster, G.; Sun, J.; Stamate, E.; Shen, B.; Rijnders, G.; Linderoth, S. *Nano Lett.* **2011**, *11*, 3774−3778.
(14) Kalabukhov, A.; Gunnarsson, R.; Börjesson, J.; Olsson, E.; Claeson, T.; Winkler, D. *Phys. Rev. B* **2007**, *75*, 121404.
(15) Zhang, L.; Zhou, X.-F.; Wang, H.-T.; Xu, J.-J.; Li, J.; Wang, E. G.; Wei, S.-H. *Phys. Rev. B* **2010**, *82*, 125412.
(16) Zhong, Z.; Xu, P. X.; Kelly, P. J. *Phys. Rev. B* **2010**, *82*, 165127.
(17) Schneider, C. W.; Esposito, M.; Marozau, I.; Conder, K.; Doebeli, M.; Hu, Y.; Mallepell, M.; Wokaun, A.; Lippert, T. *Appl. Phys. Lett.* **2010**, *97*, 192107.
(18) Huijben, M.; Rijnders, G.; Blank, D. H. A.; Bals, S.; Aert, S. V.; Verbeeck, J.; Tendeloo, G. V.; Brinkman, A.; Hilgenkamp, H. *Nat. Mater.* **2006**, *5*, 556−560.
(19) Qiao, L.; Droubay, T. C.; Varga, T.; Bowden, M. E.; Shutthanandan, V.; Zhu, Z.; Kaspar, T. C.; Chambers, S. A. *Phys. Rev. B* **2011**, *83*, 085408.
(20) Liao, Y. C.; Kopp, T.; Richter, C.; Rosch, A.; Mannhart, J. *Phys. Rev. B* **2011**, *83*, 075402.
(21) Leskelä, M.; Ritala, M. *Angew. Chem., Int. Ed.* **2003**, *42*, 5548−5554.
(22) Puurunen, R. L. *J. Appl. Phys.* **2005**, *97*, 121301.
(23) Jiang, J. C.; Pan, X. Q.; Chen, C. L. *Appl. Phys. Lett.* **1998**, *72*, 909−911.
(24) Kawasaki, M.; Takahashi, K.; Maeda, T.; Tsuchiya, R.; Shinohara, M.; Ishiyama, O.; Yonezawa, T.; Yoshimoto, M.; Koinuma, H. *Science* **1994**, *266*, 1540−1542.
(25) Koster, G.; Kropman, B. L.; Rijnders, G. J. H. M.; Blank, D. H. A.; Rogalla, H. *Appl. Phys. Lett.* **1998**, *73*, 2920−2922.
(26) Diehl, R.; Brandt, G. *Mater. Res. Bull.* **1975**, *10*, 85−90.
(27) Frederikse, H. P. R.; Hosler, W. R. *Phys. Rev.* **1967**, *161*, 822−827.
(28) Tufte, O. N.; Chapman, P. W. *Phys. Rev.* **1967**, *155*, 796−802.
(29) Kim, S. K.; Lee, S. W.; Han, J. H.; Lee, B.; Han, S.; Hwang, C. S. *Adv. Funct. Mater.* **2010**, *20*, 2989−3003.
(30) Liang, X.; Meng, Z.; Wu, W. *J. Am. Ceram. Soc.* **2004**, *87*, 2218−2222.
(31) Chen, T. L.; Li, X. M.; Wu, W. B. *J. Appl. Phys.* **2005**, *98*, 064109.
(32) Lee, S. W.; Han, J. H.; Kim, S. K.; Han, S.; Lee, W.; Hwang, C. S. *Chem. Mater.* **2011**, *23*, 976−983.
(33) Charles, T, C. *Surf. Sci. Rep.* **1997**, *27*, 1−111.
(34) Ulrike, D. *Surf. Sci. Rep.* **2003**, *48*, 53−229.
(35) Fu, Q.; Wagner, T. *Surf. Sci. Rep.* **2007**, *62*, 431−498.
(36) Goldstein, D. N.; McCormick, J. A.; George, S. M. *J. Phys. Chem. C* **2008**, *112*, 19530−19539.
(37) Elliott, S. D.; Scarel, G.; Wiemer, C.; Fanciulli, M.; Pavia, G. *Chem. Mater.* **2006**, *18*, 3764−3773.
(38) *HSC Chemistry*, 5.11 ed.; Outokumpu Research Oy: Pori, Finland.
(39) George, S. M. *Chem. Rev.* **2009**, *110*, 111−131.

(40) Son, J.; Moetakef, P.; Jalan, B.; Bierwagen, O.; Wright, N. J.; Engel-Herbert, R.; Stemmer, S. *Nat. Mater.* **2010**, *9*, 482−484.

(41) Jang, H. W.; Felker, D. A.; Bark, C. W.; Wang, Y.; Niranjan, M. K.; Nelson, C. T.; Zhang, Y.; Su, D.; Folkman, C. M.; Baek, S. H.; Lee, S.; Janicka, K.; Zhu, Y.; Pan, X. Q.; Fong, D. D.; Tsymbal, E. Y.; Rzchowski, M. S.; Eom, C. B. *Science* **2011**, *331*, 886−889.

(42) Liu, Z. Q.; Leusink, D. P.; Wang, X.; Lü, W. M.; Gopinadhan, K.; Annadi, A.; Zhao, Y. L.; Huang, X. H.; Zeng, S. W.; Huang, Z.; Srivastava, A.; Dhar, S.; Venkatesan, T.; Ariando. *Phys. Rev. Lett.* **2011**, *107*, 146802.